THE JOURNAL OF PHYSICAL CHEMISTRY C

Article

pubs.acs.org/JPCC

Band Gap Modulations in UiO Metal−Organic Frameworks

Espen Flage−Larsen, Arne Røyset, Jasmina Hafizovic Cavka, and Knut Thorshaug*

SINTEF Materials and Chemistry, P.O. Box 124 Blindern, Forskningsveien 1, N-0314 Oslo, Norway

ABSTRACT: We address the metal−organic frameworks UiO-6*x* (*x* = 6, 7, 8), their band gaps, and the changes in the band gaps upon perturbations in the metal−organic framework structures. Computational studies were performed with complementary experimental band gap measurements. Band gap modulations upon hydrogen substitutions by NH_2 and NO_2 on the organic linker, hydroxylation and dehydroxylation of the metal center, different linker lengths (*x* = 6, 7, 8), and Ti and Hf substitutions for Zr were analyzed in detail. The origin of the band gap changes was thoroughly investigated, and this work confirmed a reduction in the band gap upon NH_2 and NO_2 substitutions. Furthermore, this work explicitly illustrated that changes in the band gap were also observed by changing the coordination around the Zr atom, whereas isovalent substitutions on the metal center did not yield significant perturbations of the band gap.

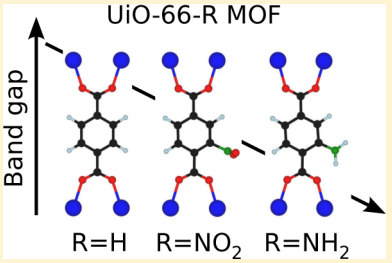

Downloaded via UNIV OF TORONTO on May 7, 2024 at 19:05:25 (UTC).
See https://pubs.acs.org/sharingguidelines for options on how to legitimately share published articles.

INTRODUCTION

Metal−organic frameworks[1] (MOFs) constitute a recently discovered class of porous materials that has received a considerable amount of attention.[2,3] In general terms, MOFs can be described as hybrid materials wherein inorganic clusters are connected by organic linkers, thereby forming regular three-dimensional structures. The vast amount of both inorganic and organic building blocks makes it possible to prepare a wide range of MOFs with interesting properties, and the potential application of MOFs within fields such as adsorption, catalysis, separation, and sensing has been reported in numerous studies.[2,3] To the best of our knowledge, the semiconducting properties of MOFs have been studied to a much lesser extent.

Among the numerous MOFs that have been reported, the UiO-66, 67, and 68 series stand out due their high stability.[4] The linkers in the UiO-MOFs (UiO-6*x*) are made from substituted dicarboxylate (*x* = 6), biphenyl dicarboxylate (*x* = 7), and terphenyl dicarboxylate (*x* = 8), whereas the inorganic fragment is a $Zr_6O_4(OH)_4$ cluster.[4] Of particular relevance to the present work are the recently reported experimental band gaps of 4.07 and 3.94 eV together with the calculated values of 4.56 and 4.19 eV for hydroxylated and dehydroxylated UiO-66, respectively.[5] The authors of that study suggested the C atoms in the linker to be the ones involved in the modulation of the band gap and that the linker thereby defines the band gap in the MOF.

Experiments have shown that the band gap in MOFs can be modified by carefully placing substituents on the organic linker or by manipulating the inorganic cluster. For instance, it was suggested by Civalleri et al.[6] that the band gap in various MOF-5 analogues may be altered by using various dicarboxylates as linkers. Furthermore, Gascon et al.[7] showed that the band gap in MOF-5 can be modified within the range of 3.3−4.0 eV by adding electron-donating substituents onto the organic linker. The authors pointed out that the semiconducting behavior of the MOF appeared to depend more on the choice of substituent than on the substitution pattern.

If we turn our attention to the inorganic cluster, Botas et al.[8] showed that the band gap in MOF-74 (CPO-27) can be modified in the range of 1.88−2.88 eV by[6] exchanging Zn atoms in pure MOF-74 with varying amounts of Mg, Cu, or Co in the inorganic cluster. On the other hand, Fuentes-Cabrera et al.[9] demonstrated by means of DFT calculations that M-IRMOF-1 (M = Be, Mg, Ca, Zn, and Cd) all have approximately the same band gaps of 3.5 eV, and thus, the corner element on the inorganic cluster does not seem to influence significantly the band gap in M-IRMOF. According to Choi et al.,[10] first-principle calculations show that a lowering of the band gaps can be achieved by exchanging Zn^{2+} ions with Co^{2+} ions without changing the organic linker in IRMOF-1. Furthermore, Kuc et al.[11] studied over 30 different IRMOFs where the organic linker was perturbed while the inorganic cluster was $(Zn_4O)^{6+}$ throughout the whole study. They found band gaps in the range of 1.31−5.49 eV. In addition, they showed that the top valence and bottom conduction bands are mostly dominated by C sp^2 states of the organic linkers.

To rationally develop new MOFs with interesting electronic properties, it is necessary to deepen the knowledge of the fundamental structure−property relations between the MOFs and the property of interest, for example, the band gap. In this paper, we aim at increasing the understanding of the factors that affect the band gap in various MOFs described as UiO-6*x*-R (*x* = 6, R = H, NH_2, and NO_2; *x* = 7, R = H; *x* = 8, R = H).

MATERIALS AND METHODS

Experimental Details. All MOFs were prepared according to previously reported procedures.[4,12] $ZrCl_4$ was stirred in a mixture of DMF and H_2O (25:1) before the proper dicarboxylic acid was added and stirred for 5−10 min. The mixture was transferred into a preheated (85 °C) oven and

Received: May 30, 2013
Revised: September 5, 2013
Published: October 1, 2013

 © 2013 American Chemical Society dx.doi.org/10.1021/jp405335q | J. Phys. Chem. C 2013, 117, 20610−20616

allowed to react for 48 h. After cooling, the product was filtered, washed with DMF, and dried. This material is labeled "as synthesized" in the rest of the paper. Solvent exchange was performed by soaking the as synthesized sample in methanol without stirring for 24 h, decanting, adding fresh methanol, leaving for another 24 h without stirring, filtering, and drying. In the following, this material is referred to as "methanol containing". Finally, a selection of MOFs were activated by heating at 150 °C under vacuum overnight and are referred to as "evacuated". All starting materials and solvents were commercially available and used as received.

Diffuse reflectance measurements (DRS) were performed on powder samples with a halogen/deuterium lamp (Hamamatsu L10290), UV−vis spectrometer (BWTek i-trometer), and fiber coupled reflectance sphere (Labsphere). For the Tauc plot[13] of $\hbar\omega f(R)$ versus photon energy $\hbar\omega$, the Kubelka−Munk function $f(R) = (1 - R)^2/2R$ was calculated from the reflectance obtained from the DRS UV−vis measurements.

Computational Details. The density functional theory (DFT) calculations were based on the Perdew−Burke−Ernzerhof (PBE)[14] exchange-correlation functional and performed using the Vienna Ab initio Simulation Package (VASP).[15,16] An energy cutoff of 600 eV with a $\vec{k}$-point sampling of 5 × 5 × 5 (3 × 3 × 3) and 3 × 3 × 3 (Γ only) for the UiO-66/67 and UiO-68 electronic structure (relaxation) calculations, respectively. All relaxations were terminated when the residual forces were less than 0.01 eV/Å. In addition, calculations employing the HSE03[17] functional (screening parameter, ω = 0.3 Å^{-1}) were performed for the UiO-66 structures with a $\vec{k}$-point sampling of 3 × 3 × 3.

RESULTS AND DISCUSSIONS

The conventional unit cells of the UiO-6*x*-R structures are cubic and can contain up to 1000 atoms depending on the configuration.[4] To simplify, we used the primitive unit cell, which is triclinic. In this configuration, the UiO-66 hydroxylated unit cell contains only 114 atoms.

The relaxed difference between the dehydroxylated and hydroxylated cluster is illustrated in Figure 1 (this is similar between all three structures) along with the different linkers for the UiO-66 structures in Figure 2. For a more in-depth discussion of the layout of the UiO-6*x* structures, please consult Cavka et al.[4]

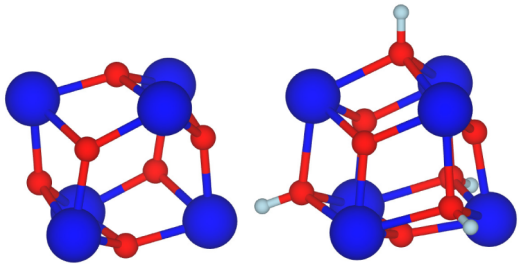

(a) (b)

Figure 1. Illustration of the dehydroxylated (a) and the hydroxylated (b) UiO-66 inorganic clusters. Colors: zirconium (blue), oxygen (red), and hydrogen (light blue).

Notice from Figure 2 that NO_2 aligns normal to the planar aromatic rings as opposed to NH_2. After the relaxation, the aromatic ring with NH_2 tended to rotate slightly (compare Figure 2, structures (a) and (b)). To accommodate both the carboxylic oxygens, the hydrogen atom on the amino group, and a lone pair of electrons in a planar conformation, such a rotation is warranted. However, for NO_2, two oxygen atoms are present and they cannot be accommodated in a similar planar conformation. The O−N−O plane formed by the NO_2 group is instead orthogonal to the aromatic rings, and thus no rotation of the aromatic ring takes place.

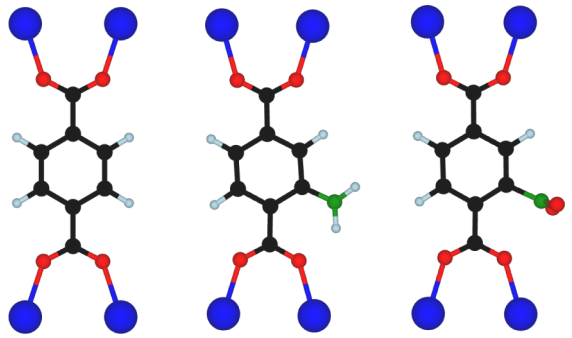

(a) H (b) NH_2 (c) NO_2

Figure 2. Linkers in the UiO-66 structure addressed in this work. Colors: Zr (blue), O (red), C (black), H (light blue), and N (green).

To investigate the band gap of the different UiO-6*x*-R compounds, their respective DFT relaxed structures were used as inputs. In addition, we synthesized a representative set of samples and performed reflectance measurements to validate our predictions. The results are summarized in Tables 1−3, and the Tauc plot used to extract the band gaps for the evacuated samples is shown in Figure 3. Our measured band gaps of 4.0−4.1 eV for the three UiO-66-H samples (as synthesized, methanol containing, and evacuated, Table 2) agree well with the band gap value of 4.07 eV measured by Valenzano et al.[5]

Table 1. Calculated Band Gaps (in eV) for the UiO-66-R Structures (R = H, NO_2, NH_2)

	dehydroxylated			hydroxylated		
	H	NH_2	NO_2	H	NH_2	NO_2
PBE	2.2	1.8	2.2	2.8	2.0	2.7
HSE03	3.3	2.2	3.4	3.9	2.7	3.8

Table 2. Experimental Band Gaps (in eV) for the Different UiO-6*x*-R (*x* = 6, 7; R = H, NO_2, NH_2) Hydroxylated Compositions

	H	NH_2	NO_2
UiO-66 evacuated	4.0	2.9	3.4
UiO-66 as synthesized	4.1	2.9	3.3
UiO-66 methanol containing	4.0	2.9	3.3
UiO-67 evacuated	3.5		
UiO-67 as synthesized	3.6		
UiO-67 methanol containing	3.6		

Table 3. Calculated Band Gaps (in eV) for the UiO-6*x* Structures (*x* = 6, 7, 8)

	dehydroxylated	hydroxylated
UiO-66	2.2	2.8
UiO-67	2.2	2.5
UiO-68	2.2	2.4

dx.doi.org/10.1021/jp405335q | J. Phys. Chem. C 2013, 117, 20610−20616

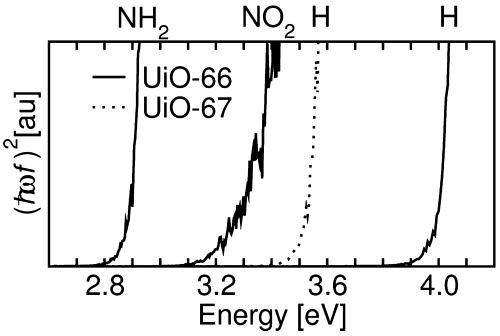

Figure 3. Tauc plot; $(\hbar\omega f)^2$ as a function of the photon energy $\hbar\omega$. The Kubelka–Munk function f was obtained from the reflectance spectra. The solid lines (UiO-66) and the dotted line (UiO-67) are given for the evacuated samples.

Furthermore, the small difference in the measured band gap between the evacuated, as synthesized, and methanol containing samples is comforting and highlights the fact that the band gaps of the UiO-6*x* structures are rather insensitive to the incorporation of these solvent molecules.

Concerning the accuracy of the absolute band gap in our calculations, we note that the numerical band gap value derived from calculations is underestimated with the PBE functional, but drastically improved by the HSE03 functional. Given the importance of incorporating exact exchange interactions in systems with significant electron transfer, such as these, this result is not surprising. Furthermore we would like to emphasize the fact that the trends observed with the PBE and HSE03 functional are similar. Because of the computational overhead, we thus opted not to perform calculations using the HSE03 functional for the UiO-67 and UiO-68 structures.

We will, in the following, discuss the results in more detail.

Hydroxylated versus Dehydroxylated Structures. From the calculated results, it is clear that, for all UiO-6*x* structures, the band gap is larger for the hydroxylated than for the dehydroxylated cluster. This can be explained by the projected density of states in Figure 4. For the hydroxylated cluster, there is no significant overlap between the O/Zr and C s-states deep in the valence band. These states are, however, interacting for the dehydroxylated cluster, leading to a split oxygen 2s peak (see lower shaded area in the top panel of Figure 4). Additional splits are seen toward the valence band maximum for the carbon states. The hydroxylated structure is more stable and has thus also the largest band gap of the two. When two H_2O molecules are removed from the structure in the transition from the hydroxylated to the dehydroxylated cluster, there are two faces on the Zr octahedron that do not contain oxygen atoms (see Figure 1). Combining such geometry with the significant electronegativity of oxygen atoms occupying the other faces likely stimulates an interaction with the carboxylate occupying octahedron sides and not from the sides without oxygen (see Figure 5a). Because of the extended range between these, the only possible interacting states possess s-state character from both the oxygen and the carbon atoms. Since the system is hybridized, these changes are also manifested in the p-states. We would like to emphasize that this interaction originates mostly from the aromatic rings in the linker and not from the carbon atoms in the carboxylate, as can be observed in Figure 5a.

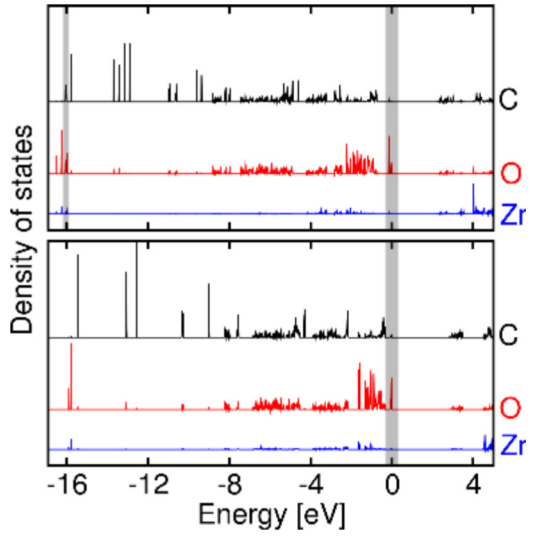

Figure 4. Projected density of states of the dehydroxylated (top panel) and hydroxylated (bottom panel) UiO-66 structure. The energy is relative to the top of the valence band. The shaded areas were used to plot projected electron density maps in Figure 5.

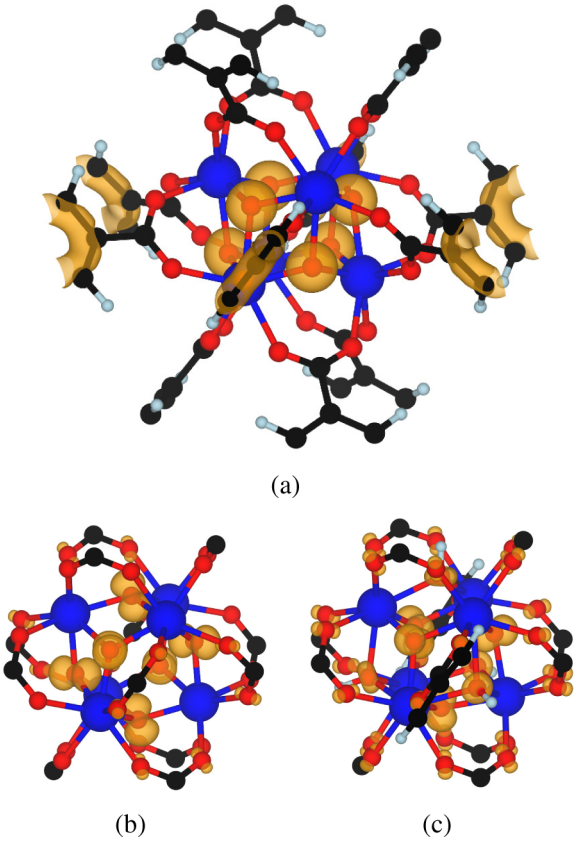

Figure 5. Projected electron density associated with the shaded areas in Figure 4 (a) dehydroxylated close to −16 eV, (b) dehydroxylated, and (c) hydroxylated, right below the top valence band. Isosurface level at 0.03 $bohr^{-3}$.

The states at the top valence band are mostly composed of nonbonding oxygen p-states containing six electrons (for both the dehydroxylated and hydroxylated clusters, see Figure 5b,c). These states are distributed throughout p-state character lobes with its axis pointing toward the center of the hydroxylated inorganic cluster. In this way, these states can lower the

dx.doi.org/10.1021/jp405335q | J. Phys. Chem. C 2013, 117, 20610−20616

interaction with the surroundings to a minimum. However, for the dehydroxylated cluster, the orbitals for these states are slightly shifted such that their axis is pointing toward the missing oxygen positions (compared to the hydroxylated cluster). This is expected in order to reduce the interaction with the aromatic rings. What is furthermore noticeable from Figure 5b,c is the lack of states from the oxygen atoms oriented in the plane of interacting carbon atoms and metal center oxygen atoms (compare Figure 5a).

For both clusters, the bottom conduction bands are very similar, composed of the aromatic linker states and the oxygen atoms on the carboxylate connected to the metal center. There is also the presence of Zr states.

In total, this leads to less bound oxygen states in the dehydroxylated cluster, and the band gap is consequently reduced.

To investigate the deficiencies of the PBE functional in DFT, we also performed calculations incorporating the HSE03 functional (see the Materials and Methods section and Table 1). Not surprisingly, this yielded a band gap in closer agreement with the experiments. In fact, it is very close to the measured band gap, in accordance with previous studies using similar functionals.[5] However, this is most likely fortuitous and it cannot be assumed that this is transferable to other systems. We would instead like to emphasize the similarities between the band gap difference of the dehydroxylated and hydroxylated cluster between the different functionals. This work primarily investigates band gap differences; thus, the HSE03 calculations add credibility to the fact that our calculated results are likely to reproduce the experimental trends.

Linker Length. It is interesting to investigate how the band gap changes when the linker length is increased. The UiO-6*x* (*x* = 6, 7, 8) structures are ideal for such investigations, as they exist with three different linker lengths (one, two, and three aromatic rings) where the inorganic cluster is unchanged. From Table 3, it is seen that the calculated band gap decreases when the linker length increases for the hydroxylated cluster. These findings are supported by the experimentally obtained band gaps for UiO-66 and UiO-67 given in Table 2, which show that the band gap in UiO-66 is higher than that in UiO-67. However, we do note a slightly larger change in the experimentally obtained band gap between the UiO-66 and UiO-67 structures compared to the calculated values.

To investigate the cause for the decrease in the band gap with an increase in the linker length, we give the projected density of states for the three structures in the hydroxylated cluster in Figure 6. It is clear that, as the linker length grows, additional carbon states appear in the top valence band. The distance from these down to the topmost carbon peak in UiO-66 increases for increasing linker length. By projecting the electron density (see Figure 7 for the UiO-68 structure) of these states, we are able to track down where they are located in the structure. They mainly reside on the carbon atoms, particularly the carbon atoms connecting the aromatic rings furthest away from the metal centers. Similar observations were also made for UiO-67.

Consequently, as the linker length grows, there will be more of these carbon states compared to the metal center states in the structure. By inspecting Figure 6, it is clear that there are additional carbon states appearing in the top valence band as the linker length grows (these are almost absent in comparison for the UiO-66 structure), which are not associated with the

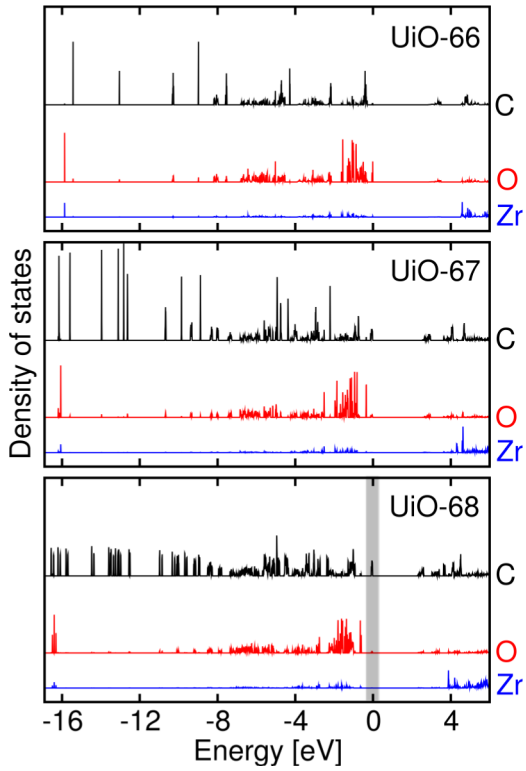

Figure 6. Projected density of states of hydroxylated UiO-66 (top panel), UiO-67 (middle panel), and UiO-68 (bottom panel). The energy is relative to the top of the valence band.

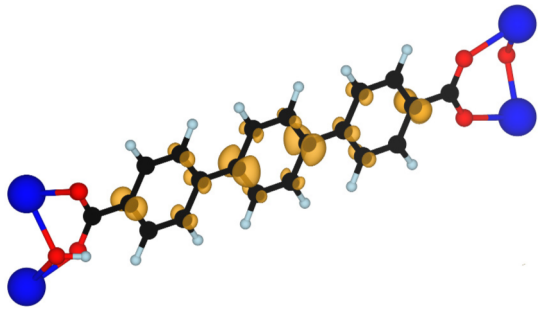

Figure 7. Projected electron density for the UiO-68 structure associated with the shaded area in the bottom panel in Figure 6. Isosurface set at 0.01 bohr^{-3}.

covalent carbon−carbon bond. These states interact, raise the valence band maximum, and thus reduce the band gap.

It is interesting to note that the calculated band gap changes are almost entirely absent for the dehydroxylated clusters as the linker length grows. The explanation is simple; the nonbonding oxygen states discussed in the previous section appear above the additional carbon states in the top valence band and thus primarily define the band gap. Upon closer investigations of the density of states for the dehydroxylated UiO-68, additional carbon states reside just above the nonbonding oxygen states, whereas, for the UiO-67, it resides just below. It is thus reasonable to assume that further linker lengthening past UiO-68 would indeed again reduce the band gap for the dehydroxylated cluster.

However, given the complexity of these systems, we consider the qualitative agreement to be satisfying. A detailed study of the alignment of the oxygen states in comparison to the carbon

dx.doi.org/10.1021/jp405335q | J. Phys. Chem. C 2013, 117, 20610−20616

states in the top valence band with more accurate post-DFT routines might shed further light on the cause of the discrepancy.

Linker Modifications. We a priori expected that, by substituting H with electron donating (e.g., NH_2) or withdrawing substituents (e.g., NO_2) on the linker, we could perturb the electron density distribution within the MOF, and thereby also influence the band gap. We, therefore, prepared the three MOFs UiO-66-R (R = H, NH_2, NO_2) and studied the optical and calculated band gaps. As seen from Tables 1 and 2, the band gaps determined from both the computations and the experiments show significant changes with changes in R.

When we compare the band gaps calculated for the hydroxylated structures in Table 1 (HSE03) and the experimentally obtained values given in Table 2, we see that the trends in the band gaps upon NH_2 and NO_2 substitution onto the aromatic rings of UiO-66 are similar for both the experiments and the computations. The trend is H > NO_2 > NH_2, where R = H shows the largest band gap. On the other hand, the trend in the Hammet σ_m parameter is NH_2 < H < NO_2,[18] where the σ_m values are −0.16, 0.00, and +0.71, respectively. Our findings are in contrast to the linear relationship between the band gap and the Hammet parameter that was reported by Gascon et al.[7] for IR-MOFs 1, 2, 7, 8, and 9, where $-0.6 < \sigma_R^0 < 0$. Although our data set only consists of three points, the data show that a linear correlation between the band gap and the Hammet parameter is not generally valid. Such linearity cannot necessarily be claimed over a wider range of σ_m and for other MOFs than the ones studied by Gascon et al.[7]

The band gap decreases when hydrogen is substituted by NH_2. Such a change is observed from both the experimentally and the computationally obtained values for the hydroxylated structures, and from the computationally obtained band gaps for the dehydroxylated structures. For the hydroxylated structures, the calculated change is 1.2 eV (HSE03) when we compare the values for R = H and R = NH_2, whereas the change is 1.1 eV (HSE03) for the dehydroxylated samples (Table 1). For the experimentally determined band gaps, the difference between the R = H and R = NH_2 values is 1.1 eV, in agreement with the 1.2 eV difference found by computations. The bonding of the substituent to the linker is similar to that of the internal bonds in the NH_2 molecule, where an sp^2 hybridization is formed. The unaccounted electron associated with nitrogen bonds to the carbon atom, and there is a remaining p-state orbital that contains the lone pair. To again track down the origin of the change in the band gap, we give the density of states and the projected electron density associated with the bands right below the Fermi level in Figure 8 (hydroxylated) and Figure 9 (dehydroxylated). For the empty configuration, the top valence band is dominated by non-bonding oxygen states that are highly delocalized, but associated with the metal center as previously discussed.

However, it is clear that the lone pair associated with the nitrogen atom resides in the top valence band. This orbital is aligned normal to the NH_2 group. Furthermore, the peak below (also shaded, see Figure 8a,b) is very similar to the delocalized metal center states of the empty configuration. The reduced band gap is thus caused by a decreased binding energy that originates from the repulsive interaction between the lone pair associated with the nitrogen atom and the delocalized metal center states. This also fully justifies the slight rotation of the ring (see Figure 2) to reduce the interaction with the closest

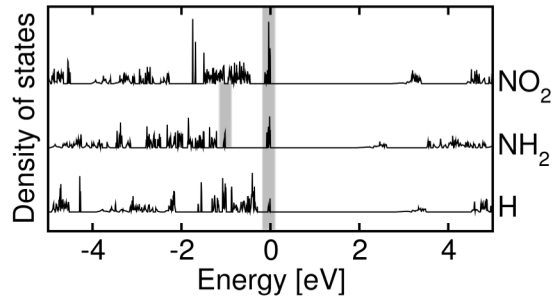

(a) Density of states

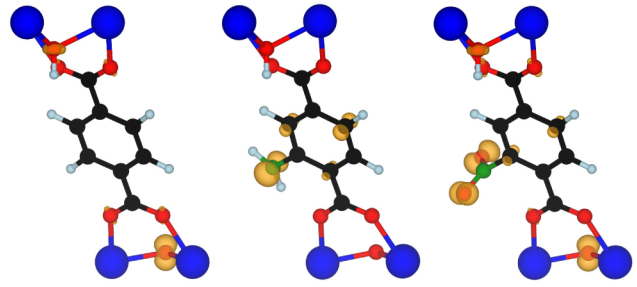

(b) H (c) NH_2 (d) NO_2

Figure 8. (a) Density of states for the hydroxylated UiO-66-R structure with R = H, NH_2, and NO_2. The projected electron density (the shaded energy range in the top valence band) is shown in (b)−(d). The second energy slit (shaded at around −1 eV) for R = NH_2 contains similar states as those projected for H in (b).

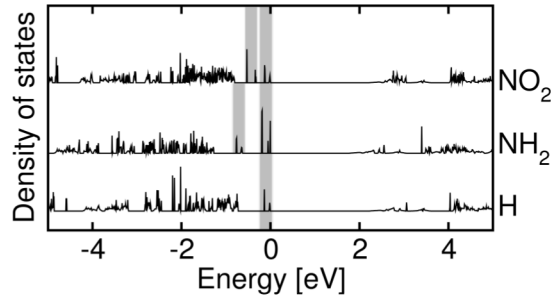

(a) Density of states

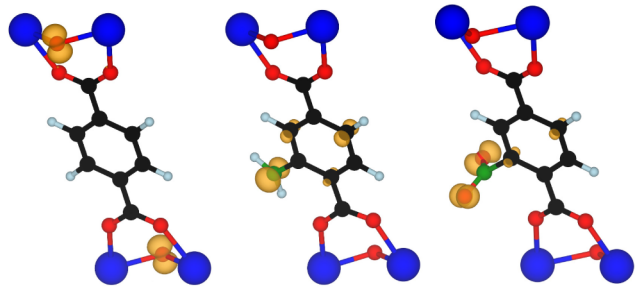

(b) H (c) NH_2 (d) NO_2

Figure 9. (a) Density of states for the dehydroxylated UiO-66 structure with R = H, NH_2, and NO_2. The projected electron density (associated with the shaded energy ranges in (a)) is shown in (b)−(d). The second energy slit (shaded at around −1 eV) for R = NH_2 contains similar states as those projected for H in (b). For R = NO_2, the topmost shaded area contains similar states as projected in (b), while (d) shows the projected states associated with the second topmost shaded area (around −0.5 eV).

dx.doi.org/10.1021/jp405335q | J. Phys. Chem. C 2013, 117, 20610−20616

oxygen atom (also containing parts of the delocalized metal center states) to a minimum.

NH_2 substitution in the hydroxylated MOF yields a larger change in the band gap compared to the dehydroxylated MOF. This can be explained by comparing the density of states in Figures 8a and 9a, where it is clear that there is a stronger interaction between the lone pair states and the delocalized metal center states for the hydroxylated MOF (compare shaded areas). The increased interaction can be explained from the previous discussion of the difference between the hydroxylated and dehydroxylated structures; in the hydroxylated clusters, the delocalized metal center states are symmetric (all NH_2 interact), whereas, for the dehydroxylated clusters, half of the aromatic linkers have a reduced projected electron density at their outermost oxygen atoms and shifted orbitals at the innermost. This is the electron density that would interact with the nitrogen lone pair states, yielding a reduced interaction between the two and less changes to the band gap.

NO_2 substitutions yield similar calculated band gaps as the model with only hydrogen atoms on the linker. This is valid for both the hydroxylated and the dehydroxylated structures. Nitrogen in NO_2 also has an unsaturated electron. It thus bonds reasonably well to carbon with all electrons saturated in bonds, and from this perspective, we should not expect a large change in the band gap. However, the oxygen atoms will have lone pairs, as can be seen in Figures 8c and 9c. The interaction between these and the delocalized metal center states is not significant (they are both present in the energy slit used in Figure 8c). This is reasonable, given their fairly large spatial separation. Correspondingly, we do not see a distortion of the aromatic ring (compare Figure 2, structures (b) and (c)) and we should not expect as large of a change in the band gap as that observed for NH_2 substitutions. This is indeed confirmed by the calculated results, where only a slight reduction in the band gap can be seen, and by the experiments for UiO-66, where we observe a 0.6 eV lowering of the band gap when we go from R = H to R = NO_2. According to the calculations, however, the lowering of the band gap is 0.1 eV. Presently, we do not have a clear explanation of this difference between the experimental and the calculated values.

We would like to emphasize the similarities between the projected electron densities of the hydroxylated and dehydroxylated clusters upon substitutions on the linker. These structures seem to behave in a rather predictable manner such that the changes due to the hydroxylation/dehydroxylation of the metal centers do not greatly affect the results of the individual substitutions on the linker and vice versa. This is a comforting fact for future electronic structure studies of these materials.

Metal Exchange in the Inorganic Cluster. Few studies have investigated substitutions in the metallic center of the UiO-66 structure. To address this, we substituted Ti and Hf for Zr in the structure and studied the MOFs by computations. For the dehydroxylated clusters, we generated structures containing Zr/Ti and Zr/Hf ratios of 5:1 and 0:6, respectively.

For the hydroxylated cluster, only ratios of 5:1 were included. These structures were then fully relaxed in order to calculate their band gaps. From Table 4, it is clear that modifications to the metal center, assuming we can do nothing with the oxygen atoms, are not yielding significant changes in the band gap for isovalent substitutions. A small decrease was seen for the complete Ti substitution. This is expected from the size differences. Previous statements[5] regarding modifications to the linker as the most fruitful route to optimize the band gap is thus supported by our study. We only investigated isovalent substitutions, and it remains to be seen what could be achieved by more drastic changes to the metal center. It must also be kept in mind that the UiO- and IR-MOFs consist of separate inorganic clusters, whereas the CPO structures contain chains of clusters.

Table 4. Calculated Band Gaps (in eV) for the UiO-66 Structure with Ti and Hf Substitutions in the Metallic Center

	dehydroxylated	hydroxylated
UiO-66(Zr/Ti)	2.2	2.8
UiO-66(Zr/Hf)	2.2	2.9
UiO-66(Ti)	2.2	2.6
UiO-66(Hf)	2.2	2.9

CONCLUSIONS

This work addressed band gap modulations of the UiO-6*x*-R (*x* = 6, R = H, NH_2, and NO_2; *x* = 7, R = H; *x* = 8, R = H) structures. We quantified the change in the band gap upon substituting H with NH_2 and NO_2 on the linker, varying the linker length, and substituting Ti and Hf for Zr in the metal center. Significant reduction of the band gap was observed by introducing NH_2 and, to a smaller extent, NO_2 in the structure. This was explained by lone-pair interaction with the bulk structure. Furthermore, we highlighted the change in the band gap upon hydroxylation versus dehydroxylation of the metal center. Hydroxylation increased the band gap, which was traced back to the fact that the dehydroxylated structure contained an oxygen−carbon interaction deep in the valence band. This interaction reduced the binding energy of the nonbonding oxygen atoms and thus reduced the band gap in the dehydroxylated structure. Finally, we provided quantitative evidence that substitutions in the metal center by isovalent elements will not yield significant changes in the band gap.

We have brought conclusive evidence of previous statements of the possibility of tuning the band gap upon introduction of functional groups on the linker and shown explicitly that the origin of the band gap changes does not exclusively relate to changes in the linker, but also to how nonbonding oxygen states interact with the states on the aromatic rings.

AUTHOR INFORMATION

Corresponding Author

*E-mail: knut.thorshaug@sintef.no.

Notes

The authors declare no competing financial interest.

ACKNOWLEDGMENTS

We gratefully acknowledge SINTEF Materials and Chemistry for financial support, the NOTUR consortium for computational resources, A. Andersen for preparing the MOFs, and O. M. Løvvik for discussion.

REFERENCES

(1) Yaghi, O. M.; Li, H. L. Hydrothermal Synthesis of a Metal−Organic Framework Containing Large Rectangular Channels. *J. Am. Chem. Soc.* **1995**, *117*, 10401−10402.

(2) Férey, G. Hybrid Porous Solids: Past, Present, Future. *Chem. Soc. Rev.* **2008**, *37*, 191−124.

(3) Cook, T. R.; Zheng, Y.-R.; Stang, P. J. Metal−Organic Frameworks and Self-Assembled Supramolecular Coordination

Complexes: Comparing and Contrasting the Design, Synthesis, and Functionality of Metal−Organic Materials. *Chem. Rev.* **2013**, *113*, 734−777.
(4) Cavka, J. H.; Jakobsen, S.; Olsbye, U.; Guillou, N.; Lamberti, C.; Bordiga, S.; Lillerud, K. P. A New Zirconium Inorganic Building Brick Forming Metal Organic Frameworks with Exceptional Stability. *J. Am. Chem. Soc.* **2008**, *130*, 13850−13851.
(5) Valenzano, L.; Civalleri, B.; Chavan, S.; Bordiga, S.; Nilsen, M. H.; Jakobsen, S.; Lillerud, K. P.; Lamberti, C. Disclosing the Complex Structure of UiO-66 Metal Organic Framework: A Synergic Combination of Experiment and Theory. *Chem. Mater.* **2011**, *23*, 1700−1718.
(6) Civalleri, B.; Napoli, F.; Noel, Y.; Roetti, C.; Dovesi, R. Ab-Initio Prediction of Materials Properties with CRYSTAL: MOF-5 as a Case Study. *Cryst. Eng. Comm.* **2006**, *8*, 364−371.
(7) Gascon, J.; Hernandez-Alonso, M. D.; Almeida, A. R.; van Klink, G. P. M.; Kapteijn, F.; Mul, G. Isoreticular MOFs as Efficient Photocatalysts with Tunable Band Gap: An Operando FTIR Study of the Photoinduced Oxidation of Propylene. *ChemSusChem* **2008**, *1*, 981−983.
(8) Botas, J.; Calleja, G.; Sanchez-Sanchez, M.; Orcajo, M. G. Effect of Zn/Co Ratio in MOF-74 Type Materials Containing Exposed Metal Sites on Their Hydrogen Adsorption Behaviour and on Their Band Gap Energy. *Int. J. Hydrogen Energy* **2011**, *36*, 10834−10844.
(9) Fuentes-Cabrera, M.; Nicholson, D. M.; Sumpter, B. G.; Widom, M. Electronic Structure and Properties of Isoreticular Metal-Organic Frameworks: The Case of *M*-IRMOF1 (*M* = Zn, Cd, Be, Mg, and Ca). *J. Chem. Phys.* **2005**, *123*, 124713.
(10) Choi, J.; Choi, Y.; Lee, J.; Shin, W.; Kang, J. Tunability of Electronic Band Gaps from Semiconducting to Metallic States via Tailoring Zn Ions in MOFs with Co Ions. *Phys. Chem. Chem. Phys.* **2009**, *11*, 628−631.
(11) Kuc, A.; Enyashin, A.; Seifert, G. Metal−Organic Frameworks: Structural, Energetic, Electronic, and Mechanical Properties. *J. Phys. Chem. B* **2007**, *111*, 8179−8186.
(12) Garibay, S. J.; Cohen, S. M. Isoreticular Synthesis and Modification of Frameworks with the UiO-66 Topology. *Chem. Commun.* **2010**, *46*, 7700−7702.
(13) Tauc, J. Optical Properties and Electronic Structure of Amorphous Ge and Si. *Mater. Res. Bull.* **1968**, *3*, 37−46.
(14) Perdew, J. P.; Burke, K.; Ernzerhof, M. Generalized Gradient Approximation Made Simple. *Phys. Rev. Lett.* **1996**, *77*, 3865−3868.
(15) Kresse, G.; Hafner, J. Ab Initio Molecular Dynamics for Liquid Metals. *Phys. Rev. B* **1993**, *47*, 558−561.
(16) Kresse, G.; Hafner, J. Ab Initio Molecular-Dynamics Simulation of the Liquid-Metal−Amorphous-Semiconductor Transition in Germanium. *Phys. Rev. B* **1994**, *49*, 14251−14269.
(17) Heyd, J.; Scuseria, G. E.; Ernzerhof, M. Hybrid Functionals Based on a Screened Coulomb Potential. *J. Chem. Phys.* **2003**, *118*, 8207−8215.
(18) Hansch, C.; Leo, A.; Taft, R. W. A Survey of Hammett Substituent Constants and Resonance and Field Parameters. *Chem. Rev.* **1991**, *91*, 165−195.